Inorg. Chem. **2002**, *41*, 967–972

Gas-Phase Photofragmentation of Tris(methyl vinyl ketone) Tungsten(0) and the Relationship to Laser-Assisted CVD of Tungsten Oxide Thin Films

Theodore W. Bitner and Jeffrey I. Zink*

Department of Chemistry and Biochemistry, University of California at Los Angeles, Los Angeles, California 90095

Received July 13, 2001

The gas-phase laser-induced photofragmentation of tris(methyl vinyl ketone) tungsten(0) is studied, and the photoproducts are identified by time-of-flight mass spectroscopy. The initially populated excited electronic state of the complex is attributed to metal-to-ligand charge transfer by analysis of the electronic and preresonance Raman spectra. The major metal-containing photofragmentation products are W^+ and WO^+; smaller amounts of WC^+ and $W(C_2H_2)^+$ are also observed. Intramolecular ligand coupling occurs, and dimeric products and their fragments are identified. Reaction pathways that explain the observed products are proposed. Thin films on silicon substrates are produced by laser-assisted chemical vapor deposition. The films consist of polycrystalline tungsten oxide with less than 10% tungsten carbide and are characterized by X-ray diffraction, SEM, and Auger electron spectroscopy. Relationships between the composition of the gas-phase photofragments and that of the solid films are discussed.

Introduction

Recent studies of the gas-phase laser photolysis of volatile transition-metal compounds have shown that heteroatoms (X) including carbon, oxygen, nitrogen, and fluorine are abstracted from the ligands in an intramolecular reaction to form the corresponding M−X species.[1−17] For example, photolysis of metal hexafluoroacetylacetonates, ($M(hfac)_n$, M = Cr, Ni, Cu, Pd, or Pt) produces diatomic metal carbides or fluorides in the gas phase.[5,7,11]

Volatile metal-containing compounds are useful precursors for laser-assisted chemical vapor deposition of important materials. The deposition of thin films routinely leads to both desired and undesired incorporation of M−X species. In some cases, these small metal fragments corrupt the quality of the films. For example, in the case of the transition-metal hexafluoroacetylacetonate complexes, the binary metal fluorides, MF, or metal carbides, MC, that were major gas-phase photofragmentation products were incorporated into the films, producing fluorine or carbon contamination.[13−17] In contrast, formation of the desired metal diatomic species such as binary metal nitrides (e.g., TiN from $Ti(NEt_2)_4$) can occur when the stoichiometry of the diatomic metal photofragment is the same as that of the desired film.[6−10]

The first goal of this work was to investigate whether the gas-phase photofragmentation of tris(methyl vinyl ketone) tungsten(0), $W(mvk)_3$, produces metal atoms, heteroatomic metal−oxygen species, or heteroatomic metal−carbon species. Because both carbon and oxygen atoms are directly

* Corresponding author. E-mail: zink@chem.ucla.edu.

(1) Jackson, R. L. *Acc. Chem. Res.* **1992**, *25*, 581.
(2) Gedanken, A.; Robin, M. B.; Kuebler, N. A. *J. Phys. Chem.* **1982**, *86*, 4096.
(3) Mikami, N.; Ohki, R.; Kido, H. *Chem. Phys.* **1990**, *141*, 431.
(4) Wilwohl, H.; Wolfrum, J. *Appl. Surf. Sci.* **1990**, *54*, 89.
(5) Muraoka, P.; Byun, D.; Zink, J. I. *J. Am. Chem. Soc.* **2000**, *122*, 1227.
(6) Cheon, J.; Guile, M.; Muraoka, P.; Zink, J. I. *Inorg. Chem.* **1999**, *38*, 2238.
(7) Talaga, D. S.; Hanna, S. D.; Zink, J. I. *Inorg. Chem.* **1998**, *37*, 2880.
(8) Cheon, J.; Zink, J. I. *Chem. Mater.* **1997**, *9*, 1208.
(9) Cheon, J.; Zink, J. I. *J. Am. Chem. Soc.* **1997**, *119*, 3838.
(10) Cheon, J.; Talaga, D. S.; Zink, J. I. *J. Am. Chem. Soc.* **1997**, *119*, 163.
(11) Talaga, D. S.; Zink, J. I. *Inorg. Chem.* **1996**, *35*, 5050.
(12) Wexler, D.; Zink, J. I.; Tutt, L.; Lunt, S. R. *J. Phys. Chem.* **1993**, *97*, 13563.
(13) Wilwohl, H.; Wolfrum, J.; Zumbach, V.; Albers, P.; Seibold, K. *J. Phys. Chem.* **1994**, *98*, 2242.
(14) Braichotte, D.; Garrido, C.; van den Bergh, H. *Appl. Surf. Sci.* **1990**, *46*, 9.
(15) Eden, J. G. *Photochemical Vapor Deposition*; Wiley & Sons: New York, 1992.
(16) Hitchman, M. L.; Jensen, K. F. *Chemical Vapor Deposition: Principles and Applications*; Academic Press: San Diego, 1993.
(17) Koidas, T. T.; Hampden-Smith, M. J. In *The Chemistry of Metal CVD*; Kodas, T. T., Hampden-Smith, M. J., Eds.; VCH: New York, 1994

10.1021/ic0107532 CCC: $22.00
Published on Web 01/31/2002

coordinated to the metal, tungsten may preferentially abstract either a carbon or an oxygen atom from the ligand. Only two gas-phase photofragmentation studies of organometallic tungsten complexes ($W(CO)_6$ and $W(\eta^6\text{-}C_6H_6)$) have been reported in the literature.[18,19] $W(mvk)_3$ is an ideal complex for a gas-phase study because it is air-stable and readily volatile. The second goal of this work was to compare the composition of the gas-phase photofragmentation products with that of the laser-assisted CVD thin film. The similarities or differences that exist between thermal chemical vapor deposition and laser deposition of thin films from $W(mvk)_3$ are also of interest.[20]

In this contribution, we examine the gas-phase photofragmentation pathways of $W(mvk)_3$ by using time-of-flight mass spectroscopy. Both carbon-atom and oxygen-atom abstraction occur. Surprisingly, the WO^+ diatomic is the most common photofragment in the mass spectrum. Equally surprisingly, ligand dimerization occurs even under collision-free conditions. The initially populated excited electronic state was assigned from absorption and resonance Raman spectroscopy data. Thin films were prepared by laser-assisted chemical vapor deposition. Analysis of the films by Auger electron spectroscopy and X-ray diffraction revealed that the films consist of crystalline WO_3 with some carbon incorporation. Gas-phase photolytic mechanisms and the relationships between the gas-phase and photodeposition reactions are discussed.

Experimental Section

Synthesis. The $W(mvk)_3$ complex was prepared following the literature method with a slight modification in the procedure.[21] The synthesis involves the preparation of $W(CO)_3(C_2H_5CN)_3$ from $W(CO)_6$, followed by reaction with methyl vinyl ketone.[22] $W(CO)_6$ (Aldrich) was purified by sublimation at 40 °C and 0.01 mmHg. Following the methods of Kubas,[23] a 10.0 g sample of $W(CO)_6$ was refluxed with propionitrile for 84 h to afford $W(CO)_3(C_2H_5CN)_3$. Following purification of the $W(CO)_3(C_2H_5CN)_3$ complex, 1.39 g (3.2 mmol) of the tricarbonyl tungsten intermediate was refluxed with 1.5 mL (18 mmol) of distilled, degassed methyl vinyl ketone (Aldrich) in 50 mL of hexane for 16−18 h. After allowing the solution to reach ambient temperature, the solvent was removed in vacuo. The crude solid was gathered on a fine-fritted filter and rinsed with diethyl ether until the washings appeared colorless. The ether solution containing the $W(mvk)_3$ was then evaporated to dryness, and the impure solid was sublimed at 90 °C and 0.01 Torr. The final product, which was recrystallized from *n*-pentane and characterized by ^{1}H NMR and elemental analysis, is air-stable for several weeks but was stored in an inert atmosphere.

Absorption Spectra. Room-temperature absorption spectra of tungsten complexes dissolved in purified cyclohexane were collected using a Shimadzu UV-260 absorption spectrometer.

Raman Spectra. Spectra were obtained at room temperature using a Spex 1401 double monochromator equipped with a RCA C31034 photomultiplier tube. Data were collected with a Stanford Research System SR400 photon counter and stored on a computer. The 514.5 nm line from a coherent I-90 argon laser and the 406.7 nm line from a coherent I-90K krypton laser were used for excitation. Typical power levels were 80−100 mW for the 514.5 nm line and 10−15 mW for the 406.7 nm line. Potassium nitrate was mixed with the $W(mvk)_3$ compound in a ratio of 1:5 wt %, respectively, for use as an internal standard. Solid samples in capillary tubes tend to burn easily, and thus to avoid problems with erroneous intensities, the solid mixture was made into pellets and rotated on a sample spinner. Excitation at frequencies that approach the absorption band also tend to burn samples quickly so that reduced power levels are necessary.

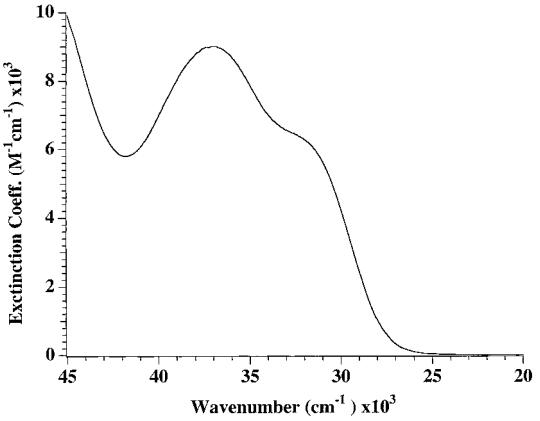

Figure 1. Room-temperature absorption spectrum of $W(mvk)_3$ in cyclohexane.

Time-of-Flight Mass Spectroscopy. The TOF mass spectrometer was constructed at UCLA. The details of this instrument are described elsewhere.[24] The sample holder was heated to the sublimation temperature of $W(mvk)_3$ (90 ± 2 °C) using high-purity helium as the carrier gas, with a backing pressure of approximately 10^3 Torr. The 308 nm line from a XeCl Lambda-Physik EMG 201 MSC operating at 20 Hz and 60 mJ/pulse was used for excitation.

Laser Photodeposition. Laser-assisted CVD was carried out at 1.70×10^{-3} Torr using a XeCl excimer laser as the excitation source while operating at 308 nm, 20 Hz, and 60 mJ/pulse. The tungsten precursor was heated in a reservoir cell to its sublimation temperature. The precursor vapor was allowed to enter the deposition chamber under dynamic vacuum conditions without the aid of a carrier gas. The laser beam was focused to a rectangular spot approximately 1 cm × 2 cm in area. The films were deposited on Si⟨100⟩ wafers that had been pretreated with 1:1 v/v ethanol/49% HF(aq). The silicon substrates were prepared at the time of the deposition experiment and were placed under vacuum. To ensure minimal atmospheric oxygen contamination following deposition, newly-deposited tungsten films were stored under an argon atmosphere.

Scanning electron microscopy and Auger electron spectroscopy measurements were made at the University of Southern California Center for Electron Microscopy Analysis. X-ray diffraction patterns were acquired using Cu Kα radiation with a power supply of 40 kV and 30 mA.

Results

1. Absorption Spectroscopy. The room-temperature absorption spectrum of $W(mvk)_3$ shown in Figure 1 contains

(18) Morse, M. D.; Geusis, M. E.; O'Brien, S. C.; Smalley, R. E. *Chem. Phys. Lett.* **1985**, *122*, 289.
(19) (a) Ishikawa, Y.; Brown, C. E.; Hackett, P. A.; Rayner, D. M. *J. Phys. Chem.* **1990**, *94*, 2404. (b) Ishikawa, Y.; Hackett, P. A.; Rayner, D. M. *J. Phys. Chem.* **1988**, *92*, 3863.
(20) Kirss, R. U.; Meda, L. *Appl. Organomet. Chem.* **1998**, *12*, 155.
(21) Schmidt, T.; Neis, S. *J. Organomet. Chem.* **1992**, *430*, C5.
(22) King, R. B.; Fronzaglia, A. *Inorg. Chem.* **1966**, *5*, 1837.
(23) Kubas, G. *Inorg. Chem.* **1983**, *22*, 692.
(24) Wiley, W. C.; McLaren, J. H. *Rev. Sci. Instrum.* **1955**, *26*, 1150.

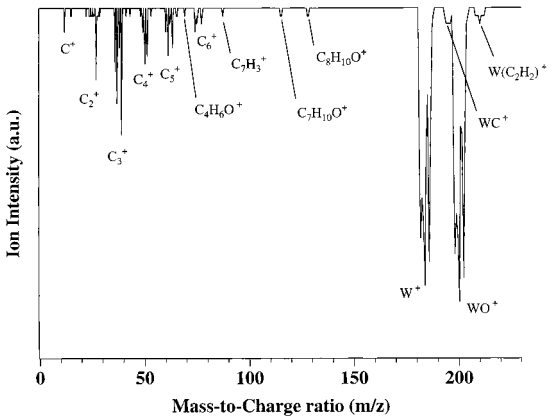

Figure 2. Time-of-flight mass spectrum of W(mvk)$_3$ from 308 nm excimer laser excitation.

Table 1. Preresonance Raman Intensities and Dimensionless Normal Mode Distortions of W(mvk)$_3$ at 406.7 nm Excitation

$\hbar w$ (cm^{-1})	I_i/I_{ref}	Δ_i/Δ_{ref}
132	0.168	2.84
364	0.0750	0.689
376	0.169	1.00
409	0.138	0.800
1366	0.0877	0.198
1538	0.0986	0.187

a band with a peak at 37 040 cm^{-1} with an extinction coefficient of 9100 M^{-1} cm^{-1}; a shoulder at approximately 31 750 cm^{-1} has an extinction coefficient of 6300 M^{-1} cm^{-1}. The values for the high-energy absorption-peak maximum and extinction coefficient agree with the previously reported values of 36 760 cm^{-1} and 9000 M^{-1} cm^{-1}, respectively.[22] Values for the shoulder were not previously reported. Excitation within either of the observed absorption bands did not produce luminescence at room temperature or at low temperature.

2. Raman Spectroscopy. The preresonance Raman intensities and frequencies that play an important role in the subsequent discussion are listed in Table 1. The numerical factors of importance in assigning the initially populated excited electronic state are the relative intensities of the normal modes I_k, which are related to the excited-state distortions Δ_k multiplied by the vibrational frequencies ω_k; therefore, $I_k = \Delta_k^2\omega_k^2$. The normal modes with the largest I_k/ω_k^2 values in the W(mvk)$_3$ complex are associated with the 132, 198, 364, 376, 409, 1366, and 1538 cm^{-1} vibrations.

3. Time-of-Flight Mass Spectroscopy. A time-of-flight mass spectrum obtained using 308 nm excitation pulses is shown in Figure 2. The mass-to-charge (m/z) ratios are listed in Table 2. The most intense peaks are observed at mass-to-charge ratios of 182, 184, 186, 198, 200, and 202. Weak, unresolved peaks centered at 196 m/z and 210 m/z are observed in the spectrum.

The ion peaks produced in the 182−210 m/z range have an apparent 2.0 ± 0.2 photon power dependence, while the mass peaks from 12 to 128 m/z have a 3.0 ± 0.2 photon power dependence. The same photon power dependencies in the TOF mass spectra were also observed when fragmentation was achieved by using 355 nm excitation from a pulsed Nd:YAG laser.

Table 2. Time-of-Flight Mass Peaks Observed from 308 nm Excitation of W(mvk)$_3$

ion (m/z)	mass fragment	ion (m/z)	mass fragment
12	C^+	60	C_5^+
15	CH^+	61	C_5H^+
27	$C_2H_3^+$	62	$C_5H_2^+$
29	$C_2H_3^+$	63	$C_5H_3^+$
36	C_3^+	65	$C_5H_5^+$
37	C_3H^+	70	$C_4H_6O^+$
38	$C_3H_2^+$	74	$C_6H_2^+$
39	$C_3H_3^+$	75	$C_6H_3^+$
41	C_2HO^+, $C_3H_5^+$	77	$C_6H_4^+$
43	$C_2H_3O^+$, $C_3H_7^+$	87	$C_7H_3^+$
48	C_4^+	116	$C_7H_{10}O^+$
49	C_4H^+	128	$C_8H_{10}O^+$
50	$C_4H_2^+$	182−186[a]	$^{182,184,186}W^+$
51	$C_4H_3^+$	196	$^{184}W\ ^{12}C^+$
53	$C_4H_5^+$	198−202	$^{182,184,186}W\ ^{16}O^+$
		210	$^{184}W(^{12}C_2\ ^1H_2)^+$

[a] The relative isotopic abundance of tungsten ^{182}W/ ^{184}W/ ^{186}W is 0.857: 1.00:0.932.

4. Thin Film Photodeposition. A scanning electron micrograph of the film surface that was deposited using 308 nm laser excitation does not show particulate or irregular surface features on the observed length scale. The deposits have reflective surfaces with a blue-to-gray metallic appearance. Newly made thin films adhere strongly enough to the surface to pass the Scotch tape test.

Auger electron spectroscopic analysis of the film's composition reveals that only tungsten (30.37%), oxygen (60.13%), and carbon (9.50%) are present. A series of depth-profile analyses by argon-ion milling over 1 min intervals (each interval corresponds to approximately 5−10 nm in depth) showed consistent atomic ratios for tungsten, oxygen, and carbon.

The X-ray diffraction patterns of the films show evidence of crystallinity. Diffraction peaks due to the tungsten oxide films were observed only at $2\theta = 21.05$ and 23.75°. A diffraction peak from the silicon substrate was observed at $2\theta = 28.80°$.

Discussion

1. Assignment of the Initially Populated Electronic State. The electronic absorption spectrum displayed in Figure 1 shows a broad band with a low-energy shoulder in the near-UV/vis wavelength region. The value of the extinction coefficient (6300 M^{-1} cm^{-1}) suggests that the lowest-energy excited electronic state originates from a charge-transfer transition, probably a metal-to-ligand charge transfer from the zerovalent metal to an empty π antibonding orbital on the ligand.

Support for this assignment is provided by the preresonance Raman intensities that are related to the bond-length changes that occur when the excited state is populated.[25] In a metal-to-ligand charge-transfer transition, bond lengths between atoms on the ligand and also between the metal and ligand atoms change. Relative excited-state bond distortions are calculated from the relative preresonance intensities

(25) Zink, J. I.; Kim-Shin, K. S. In *Advances in Photochemistry*; Volman, D. H., Hammond, G. S., Necker, D. C., Ed.; Wiley & Sons: New York, 1991; Vol. 16, p 119.

using Savin's formula.[26] The most intense normal modes along with the calculated excited-state dimensionless distortions are the 132 cm^{-1}, $\Delta = 2.84$; 364 cm^{-1}, $\Delta = 0.69$; 376 cm^{-1}, $\Delta = 1.00$; 409 cm^{-1}, $\Delta = 0.80$; 1366 cm^{-1}, $\Delta = 0.20$; and 1538 cm^{-1}, $\Delta = 0.19$ vibrations. It is evident that the initially populated excited-energy electronic state involves changes in both metal-to-ligand normal modes (in the 300−500 cm^{-1} frequency range) and higher-frequency ligand-centered modes. The distortions in both metal-to-ligand and ligand-centered vibrational modes support the assignment of the lowest-energy excited electronic state to a charge-transfer transition that most likely involves the $W(d_\pi) \rightarrow mvk(\pi^*)$ molecular orbitals.

2. Time-of-Flight Mass Spectroscopy. Gas-phase photolysis of $W(mvk)_3$ at 308 nm produces many photofragments of significant intensity, with mass peaks ranging from those of individual ligand atoms to metal-containing species with *m*/*z* values greater than 200. As expected, one major fragment is the bare metal ion; weak metal−ligand bonds are readily broken, and photofragments from the free ligand and the bare metal ion are abundant. Also as expected, there are large numbers of light species resulting from multiphoton fragmentation of both the ligand and pieces of the ligand. The intact molecular ion is not observed. Unexpectedly, the major species is the diatomic tungsten oxide ion. Very surprisingly, ligand-coupling products are observed.

A. Expected Photofragments. The intense ion peaks in the mass spectrum at 182−186 *m*/*z* arise from the isotopes of tungsten, W^+. Metal-ion peaks are frequently the most intense peaks in the mass spectra of metal complexes that undergo multiphoton ionization by intense laser pulses.[1] Metal−ligand bonds (especially those involving organic ligands) are often much weaker than C−C and C−O bonds in the ligands themselves. Extensive metal−ligand photofragmentation followed by photoionization is common, and metal-ion peaks are ubiquitous in the multiphoton ionization mass spectra of organometallic compounds.

Many well-resolved peaks over the range of 12−53 *m*/*z* arise from extensive photofragmentation of the methyl vinyl ketone ligand. These photofragments primarily consist of C−H species ranging from an atomic carbon ion (C^+) to $C_4H_5^+$, with a few oxygen-containing species also present. In addition to the lighter ligand photofragments, a mass peak is observed at 70 *m*/*z*, corresponding to the photoionized intact ligand.

The mass peaks from 12 to 128 *m*/*z*, originating from ligand photofragmentation, follow an apparent three-photon power law. The total energy of three 308 nm photons (12.05 eV) is not enough to cleave the ligand-centered bonds and produce small fragments such as C^+ or C_2^+. Typical dissociation energies for the bonds in the methyl vinyl ketone ligand are 3.596 (C−C), 6.363 (C═C), 8.281 (C═O), 3.710 (C−O), and 4.281 eV (C−H).[27] Saturation effects such as those observed here are common in multiphoton mass spectroscopy. When saturation occurs, the number of photons predicted from the observed power law is smaller than the actual number of photons necessary for the process.

B. Unexpected Photofragments. Mass peaks that do not correspond to small fragments from the ligand are observed at mass-to-charge values of 60−128 *m*/*z*. These mass peaks are the result of photoinduced coupling reactions between two ligands. This result is surprising considering the collision-free conditions in the molecular beam and is probably the consequence of intramolecular reactions between two ligands bonded to the metal. Vinyl ketone hydrocarbons are known to photopolymerize to form polymeric substances. During the thermal CVD of W thin films from this compound, oligomeric species that formed from the thermal reaction byproducts were identified by mass spectroscopy.[20] The collision-free molecular beam environment suggests that in the excited metal complex the polymerizable vinyl groups of adjacent ligands react to form dimeric species. The mass peaks at 116 and 128 *m*/*z* corresponding to $C_7H_{10}O^+$ and $C_8H_{10}O^+$, respectively, are noteworthy examples in the mass spectrum of this unexpected excited-state interaction.

The second unexpected result is that the most intense ion peaks in the mass spectrum at 198−202 *m*/*z* are from WO^+. (The cluster of peaks follows the isotopic distribution pattern of tungsten.) As discussed above, only the bare metal ion was expected to be seen in the spectrum. In addition to WO^+, a weak, unresolved peak at 196 *m*/*z* shows that the diatomic metal carbide WC^+ is formed, and weak, poorly resolved peaks centered at 210 *m*/*z* correspond to a $W(C_2H_2)^+$ molecular fragment. Photochemical mechanisms that explain the formation of both the expected and unexpected species are discussed in the next section.

Atom abstraction from metal-containing complexes in the gas phase to form diatomic species has been recently observed.[1−17] In the case of the hexafluoroacetylacetonate complexes, the diatomic metal fluoride, MF, is formed from the Cr, Cu, and Ni complexes, while the diatomic metal carbide, MC, is formed from the Pd and Pt complexes.[5,7,11] The diatomic metal nitride, MN, has also been observed from gas-phase photolysis of $Ti(NEt_2)_4$ and $Zr(NEt_2)_4$.[6]

3. Photolytic Pathways. The identities of the photofragments observed by mass spectroscopy provide information about the possible photochemical reaction pathways. Three possible photochemical pathways that lead to the formation of the unexpected photofragments are shown in Figure 3. The metal−ligand bonding that is shown in Figure 3 is based on the interpretation of the molecular structure that was determined by X-ray crystallography. The ligand bond lengths in the $W(mvk)_3$ complex are best described by a C_2═C_3 double bond and σ-type bonding of carbon and oxygen

(26) Savin's formula is given by the equation

$$\frac{I_k}{I_{k'}} = \frac{\Delta_k^2 \omega_k^2}{\Delta_{k'}^2 \omega_{k'}^2}$$

where I_k is the resonance Raman intensity, Δ_k is the dimensionless bond distortion, and ω_k is the vibrational frequency of the *k*th mode. The relative bond distortions of the *k*th mode are determined by normalizing the resonance Raman intensities with respect to the *k*′ th mode.

(27) Silverstein, R. M.; Bassler, G. C.; Morrill, T. C. *Spectrometric Identification of Organic Compounds*, 5th ed.; Wiley & Sons: New York, 1991.

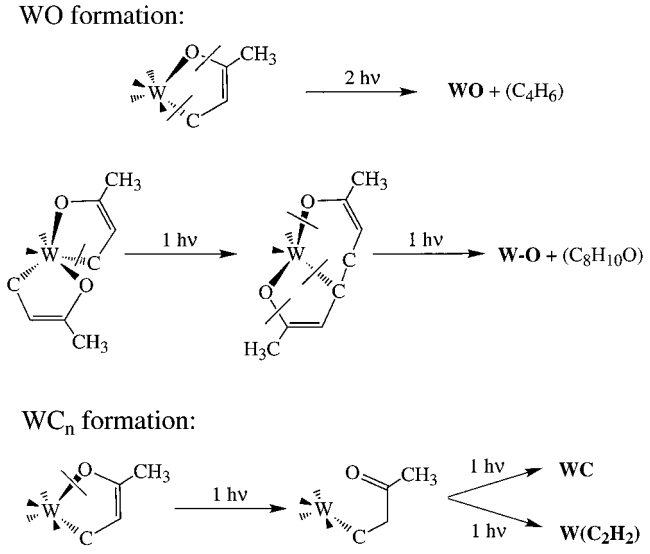

Figure 3. Photofragmentation pathways showing possible routes for production of WO^+ (top), ligand-coupling products and WO^+ (middle), and fragments containing both tungsten and carbon (bottom).

to the metal (rather than the Dewar−Chatt−Duncanson type of side-on bonding).[28]

A. Tungsten Ion Formation. Formation of bare tungsten atoms and ions probably follows a simple ligand-dissociation pathway involving multiple sequential photons. In some tungsten complexes, the low-energy excited electronic states have a dissociative potential-energy surface.[29] In addition, some metal complexes are known to have dissociative electronic states that are higher in energy than the lowest bound excited state when the molecule is in its equilibrium ground-state geometry. These higher-energy dissociative electronic states can vibronically couple to and cross below the bound state to become the lowest-energy excited state as the metal−ligand bonds lengthen.[30,31] The result is efficient photofragmentation. The details of the successive dissociation steps in the $W(mvk)_3$ complex are not known, but both directly dissociative potential-energy surfaces as well as the crossing to such surfaces could promote efficient multiphoton metal−ligand bond cleavage.

B. WO^+ Formation. The most intense peak in the mass spectrum is from the WO^+ ion. The simplest mechanism for its formation is shown in the top line of Figure 3. In this case, C−O bond cleavage is favored over W−O bond cleavage, and both tungsten oxide and C_4 fragments are produced. The bond dissociation energy of WO is 6.975 eV, but the bond dissociation energy of WC is 4.975 eV.[32−37] The stronger WO bond may explain, in part, why WO is formed preferentially over WC. WO could also be formed through a photochemical pathway that leads to the formation of the ligand-coupling products, as discussed in the next section.

C. Ligand-Coupling Reactions. Observations of C_8 species and of fragments with more than four carbons in the mvk ligand are unexpected because only intact ligands and fragments produced from intact ligands have been found in prior studies of multiphoton fragmentation of organometallic compounds. Under the collision-free conditions of the experiment, the ligand-coupling products must be formed by intramolecular reactions of partially coordinated ligands. The first steps in this pathway may involve W−C dissociation, followed by a migratory insertion-type rearrangement to form a C−C bond. This photoinitiated coupling reaction produces a dimeric C_8 species. The heaviest coupling product observed in the mass spectrum is $C_8H_{10}O^+$; the formation of this species may involve a C−O dissociation that also produces some of the observed WO^+species. The C_8^+ species can be subsequently photofragmented to produce the C_5, C_6, and C_7 species that are also observed in the TOF mass spectrum.

D. Fragments Containing Both Tungsten and Carbon. The photochemical pathways involving formation of WC^+ and $W(C_2H_2)^+$ most likely commence after cleavage of a W−O bond. At this point in the photochemical process, the partially dissociated complex may follow either of the two routes shown at the bottom of Figure 3. As a result of the cleavage, the bond order between C_2 and C_3 changes from a formal double bond to a single bond, as shown in the Figure. Formation of WC^+ would require the terminal-ligand C−C bond to be broken while formation of $W(C_2H_2)^+$ would require bond cleavage of C_2 and C_3. These two photochemical pathways are apparently less important than those originating from W−O bond cleavage, as evidenced by the significantly larger amount of WO^+ ion that is observed in the mass spectrum.

4. Laser-Assisted Deposition of Thin Films. Thin films of tungsten (VI) oxide are technologically useful materials and have applications in electrochromic displays[38−43] and thin-film NO_x gas sensors.[44−48] However, carbon contamina-

(28) Moriarty, R. E.; Ernst, R. D.; Bau, R. *J. Chem. Soc., Chem. Commun.* **1972**, 1242.
(29) (a) Lees, A. J.; Fobare, J. M.; Mattimore, E. F. *Inorg. Chem.* **1984**, *23*, 2709. (b) Zulu, M. M.; Lees, A. J. *Inorg. Chem.* **1988**, *27*, 1139. (c) Zulu, M. M.; Lees, A. J. *Inorg. Chem.* **1989**, *28*, 85.
(30) (a) Pollak, C.; Rosa, A.; Baerends, E. J. *J. Am. Chem. Soc.* **1997**, *119*, 7324. (b) Rosa, A.; Baerends, E. J.; van Gisbergen, S. J. A.; van Lenthe, E.; Groeneveld, J. A.; Snijders, J. G. *J. Am. Chem. Soc.* **1999**, *121*, 10356. (c) Baerends, E. J.; Rosa, A. *Coord. Chem. Rev.* **1998**, *177*, 97.
(31) Wilms, M. P.; Baerends, E. J.; Rosa, A.; Stufkens, D. J. *Inorg. Chem.* **1997**, *36*, 1541.
(32) Glidewell, C. *Inorg. Chim. Acta* **1977**, *24*, 149.
(33) *Experimental Chemical Thermodynamics: Combustion Calorimetry* Sunner, S.; Månsoon, M., Eds.; Pergamon Press: New York, 1979; Vol. 1, p 225.
(34) Samilova, A. N.; Efremov, Yu. M.; Gurvich, L. V. *J. Mol. Spectrosc.* **1981**, *86*, 1.
(35) Kuzyakov, Yu. Ya.; Moskvitina, E. N.; Filippova, E. N. *Spectrosc. Lett.* **1997**, *30*, 1057.
(36) Pedley, J. B.; Marshall, E. M. *J. Phys. Chem. Ref. Data* **1983**, *12*, 967.
(37) Suarez, C. B. *Spectrosc. Lett.* **1986**, *19*, 705.
(38) Baxter, D. V.; Chisolm, M. H.; Doherty, S.; Gruhn, N. E. *Chem. Commun.* **1996**, 1129.
(39) Gogova, D.; Iossifova, A.; Ivanova, T.; Dimitrova, Zl.; Gesheva, K. *J. Cryst. Growth* **1999**, *198*, 1230.
(40) Granqvist, C. G. *Electrochim. Acta* **1999**, *44*, 3005.
(41) Henley, W. B.; Sacks, G. J. *J. Electrochem. Soc.* **1997**, *144*, 1045.
(42) Maruyama, T.; Susumu, A. *J. Electrochem. Soc.* **1021**, *141*, 1021.
(43) Maruyama, T.; Kanagawa, T. *J. Electrochem. Soc.* **1994**, *141*, 2435.
(44) Chu, W. C.; Deen, M. J.; Hill, R. H. *J. Electrochem. Soc.* **1998**, *145*, 4219.
(45) DiGiulio, M.; Manno, D.; Micocci, G.; Serra, A.; Tepore, A. *J. Phys. D: Appl. Phys.* **1997**, *30*, 3211.

tion reduces the overall quality and number of potential applications of thin films.

To examine the relationship between the gas-phase photoproducts and the composition of solid thin films that are the product of laser-assisted CVD, films were produced and analyzed. In the following sections, the properties and compositions of the films and the relationships to the gas-phase photofragments are discussed.

A. Film Characterization. The WO_3 films are shiny and reflective with a blue-gray metallic appearance. They adhere slightly to the silicon substrate and pass the Scotch tape test. The SEM micrograph shows that the surface is smooth, without obvious cracks. X-ray diffraction analysis shows that the films consist of polycrystalline WO_3 and WC_{1-x}. The ⟨100⟩ diffraction peak of cubic-phase WO_3 is observed at 23.75° (23.96° JCPDS); the ⟨200⟩ diffraction peak of cubic-phase WC_{1-x} is observed at 21.05° (21.44° JCPDS). Both of the observed diffraction peaks correspond to the most intense signals from the standard crystals.

Compositional analysis of the films by Auger electron spectroscopy (AES) shows that only tungsten (30.4%), oxygen (60.1%), and carbon (9.50%) are present. These concentrations correspond to 1:3 W/O and 1:0.94 W/C. The atomic ratios remain constant throughout the film, as shown by argon-ion milling and a series of depth-profile analyses.

B. Relationship between Gas-Phase Photofragments and Thin-Film Composition. The TOF mass spectrum shows that diatomic tungsten oxide (1:1 W/O) is the primary metal-containing photofragment, while the deposited thin films have 1:3 W/O. The propensity of tungsten to bind oxygen partially explains why the oxide rather than the pure metal is deposited, but the difference in the W/O stoichiometry implies that additional sources of oxygen abstraction must be present in the surface photochemical reactions. LCVD involves a complex series of processes, including surface photochemical and photothermal reactions in addition to the gas-phase reactions that are probed in the laser photofragmentation studies. Note that the mass spectroscopy experiments detect positive ions (not neutral atoms or negative ions) and do not show the presence of oxygen atoms or ions. It is probable that these oxygen species are present in the gas phase and also contribute to the formation of the final film.

In the gas phase, fragments that contain both tungsten and carbon are observed. The WC^+ and $W(C_2H_2)^+$ photofragments found in the TOF mass spectrum are possible sources of the carbon contamination that is measured in the deposited thin films. It is interesting to note that the M−C ion signals have relative integrated intensities of 8.93 and 10.0% for WC^+ and $W(C_2H_2)^+$, respectively, with respect to the WO^+ intensity. The average M−C photofragment intensity of 9.48% closely agrees with the 9.50% atomic carbon concentration measured for the films. This similarity may be somewhat fortuitous, but the fact that W−C species are formed intramolecularly in the gas phase in the absence of surface reactions suggests that carbon contamination is an intrinsic part of the photochemistry and that it is not just a result of ligand fragments reacting with freshly deposited solid.

Summary

Photofragmentation of $W(mvk)_3$ by 308 nm laser excitation in the gas phase produces the expected bare metal ion and a variety of carbon-containing fragments; however, it also produces unexpected species such as the diatomic metal oxide ion and ligand-coupling products such as C_8 species from C_4 ligands. The metal oxide ion photoproduct is the major species present in the mass spectrum. The first photon in the multiphoton process populates a metal-to-ligand charge-transfer state; subsequent photons cause extensive fragmentation and ionization. Energetic considerations suggest that the experimentally observed power laws include saturation effects. The ligand-coupling products are formed by intramolecular reactions on the tungsten complex under the collision-free conditions of the molecular beam. Thin films produced by laser-assisted chemical vapor deposition consist of polycrystalline tungsten oxide and tungsten carbide, in contrast to metallic tungsten films that are produced by thermal CVD. The propensity of the metal in the photoexcited tungsten compound to abstract oxygen from the ligand in the gas phase suggests that the oxygen in the final film results, at least in part, from photochemical reactions. Carbon contamination of the film may be related to the smaller number of gas-phase ions containing WC. Gas-phase photolysis produces significant amounts of bare tungsten, as expected from excitation of a compound with relatively weak M−L bonds, but the results show that bond-breaking within the ligand with retention of M−L bonding is a major photochemical process.

Acknowledgment. This work was funded by a grant from the National Science Foundation (CHE98-16552).

IC0107532

(46) Manno, D.; Serra, A.; DiGiulio, M.; Micocci, G.; Tepore, A. *Thin Solid Films* **1998**, *324*, 44.
(47) Penza, M.; Tagliente, M. A.; Mirehghi, L.; Gerardi, C.; Martucci, C.; Cassano, G. *Sens. Actuators, B* **1998**, *50*, 9.
(48) Ozin, G. A.; Özkar, S. *J. Phys. Chem.* **1990**, *94*, 7556.